Sustaining metal-organic frameworks for water-gas shift catalysis by non-thermal plasma

Xu, S., Chansai, S., Stere, C., Inceesungvorn, B., Goguet, A., Wangkawong, K. W., Taylor, R., Al-Janabi, N., Hardacre, C., Martin, P. A., & Xiaolei, F. (2019). Sustaining metal-organic frameworks for water-gas shift catalysis by non-thermal plasma. *Nature Catalysis*, *2*, 142. Advance online publication. https://doi.org/10.1038/s41929-018-0206-2

Published in:
Nature Catalysis

Document Version:
Peer reviewed version

Queen's University Belfast - Research Portal:
Link to publication record in Queen's University Belfast Research Portal

Sustaining metal-organic frameworks for water-gas shift catalysis by non-thermal plasma

Shaojun Xu[1], Sarayute Chansai[1,†], Cristina Stere[1,†], Burapat Inceesungvorn[2,§], Alexandre Goguet[3,§], Kanlayawat Wangkawong[1,2], S. F. Rebecca Taylor[1], Nadeen Al-Janabi[1], Christopher Hardacre[1], Philip A. Martin[1], & Xiaolei Fan[1]

The limited thermal and water stability of metal-organic frameworks (MOFs) often restricts their applications in conventional catalysis involving thermal treatment and/or use of water. Non-thermal plasma (NTP) is a promising technique that can overcome barriers in conventional catalysis. Here we report an example of NTP-activated water-gas shift reaction (WGSR) over a MOF (HKUST-1). Significantly, the exceptional stability of HKUST-1 has been sustained under NTP activation and in the presence of water, leading to a high specific rate of 8.8 h^{-1}. We found that NTP-induced water dissociation has a two-fold promotion effect in WGSR, facilitating WGSR by supplying OH, and sustaining the stability and hence activity of HKUST-1. In situ characterisation of HKUST-1 revealed the critical role of open Cu sites in the binding of substrate molecules. This study paves the way for utilising MOFs for a wider range of catalysis.

Metal-organic frameworks (MOFs)[1], are crystalline porous materials constructed by connecting metal ions/clusters with multi-dentate organic ligands. Highly dispersed and uniformly distributed metal sites can be tailored at present in MOFs, endowing them the capacity for various

[1]School of Chemical Engineering and Analytical Science, University of Manchester, Manchester M13 9PL, United Kingdom. [2]Department of Chemistry, Faculty of Science, Chiang Mai University, Thailand, 50200. [3]School of Chemistry and Chemical Engineering, Queen's University Belfast, Belfast BT9 5AG, United Kingdom. [†]S.C. and C.S. have equal contributions to this work. [§]B.I. and A.G, have equal contributions to this work. [*]e-mail: c.hardacre@manchester.ac.uk; philip.martin@manchester.ac.uk; xiaolei.fan@manchester.ac.uk

applications, such as gas adsorption, substrate binding and heterogeneous catalysis[2, 3]. MOFs containing open metal sites (OMSs, i.e. coordinatively unsaturated metal sites) have shown great promise for optimal guest binding[4], resulting in desirable adsorption and catalysis. For example, HKUST-1, a copper benzene-1,3,5-tricarboxylate framework[5, 6], contains well-defined dimeric Cu(II) OMSs (as Lewis-acid catalysts), favouring selective binding of guest molecules for catalytic cyclisation and isomerisation reactions[7, 8]. Despite the remarkable porous nature and highly dispersed metal sites of MOFs, their practical use in conventional thermal-catalytic processes remains debatable, primarily due to the limited stability of MOFs toward heating and moisture[2, 6, 9, 10]. Non-thermal plasma (NTP)-catalysis can enable the activation of surface catalysed reactions under ambient conditions[11] and is attracting increasing attention to promote thermodynamically challenging reactions such as the water-gas-shift reaction (WGSR)[12], methane oxidation[13] and CO_2 conversion[14]. NTP has the major advantage of being able to generate highly active species and electrons (with mean electron energy of 1–10 eV) to excite molecular species as well as breaking chemical bonds under ambient conditions. Taking the conversion of CO_2 as an example, only 5.5 eV (readily achievable by NTP) is required to break the C=O bond via stepwise vibrational excitation, while a very high temperature of >1,000 °C is needed by thermal activation to dissociate CO_2 into CO and O_2 in the gas phase[14]. Therefore, NTP has the unique feature of achieving low-temperature activation of catalytic processes, which can benefit MOF-catalysis critically. Additionally, NTP can split water under ambient conditions even in the absence of a catalyst[15, 16]. This thus overcomes another major barrier of MOFs-catalysis involving moisture by impeding the water-MOFs interaction, and hence sustaining the stability of MOFs in the presence of water. There are emerging reports on the use of plasma for the surface[15, 17, 18] and structure modification[19, 20] of MOFs, as well as reactive adsorption with MOFs[21, 22]. However, a plasma-assisted MOFs-catalysed heterogeneous reaction involving water as the reactant has not been attempted, to date.

Herein, we showcase the use of NTP to promote the activity and stability of MOFs in a OMSs catalysed reaction in the presence of water. We employ the widely-reported water-unstable

MOF (HKUST-1) to catalyse WGSR at atmospheric pressure, using non-thermal argon (Ar) plasma in a packed-bed (PB) reactor[23]. We observed a notable enhancement of the stability and activity (ca. a factor of eight regarding the CO conversion) of HKUST-1 in WGSR activated by NTP in comparison to the thermal activation. The surprisingly high stability and the promoting role of HKUST-1 in the WGSR have been inferred via X-ray diffraction (XRD) and in situ optical emission spectroscopic (OES) experiments. In situ diffuse reflectance infrared Fourier transform spectroscopy (DRIFTS) studies revealed the binding of the substrate molecules (via in situ redox transition of Cu(II) to Cu(I)) and catalytic surface reactions over Cu OMSs in NTP. Importantly, no apparent loss on the crystallinity and porosity of HKUST-1 was observed post the reaction, demonstrating the potential application of HKUST-1 in a wider range of heterogeneous catalysis under similar conditions.

Results

Ar non-thermal plasma treatment of HKUST-1. The stability of MOFs (hence the retention of the active sites in a periodic arrangement) is of paramount importance to sustain their performance in catalysis. Firstly, we studied the stability of HKUST-1 in the plasma via the NTP activation of water-saturated HKUST-1 in a PB Plasma (PBP, Supplementary Fig. 1) reactor. The strong affinity of OMSs for water molecules in HKUST-1 results in catalyst deactivation[2] and poor hydrothermal stability[6, 9, 10] upon exposure to moisture. Recent work showed that oxygen (O_2) plasma could remove the coordinated water molecules from HKUST-1[15], but the highly oxidative O_2 plasma damaged the MOF as well. We found that ambient Ar NTP was capable of activating the HKUST-1 sample effectively by dissociating the chemisorbed water from OMSs but retaining its porous network. The in-line analysis of evolved gases from a PBP reactor with wet HKUST-1 pellets showed the evolution of H_2 and O_2 (with the molar volume ratio of 2.0 ± 0.16, Fig. 1a). Infrared (IR) vibrational spectroscopic study of plasma treated HKUST-1 also verified the elimination of the water molecules bonded with OMSs (Supplementary Figs. 2 and 3).

Moreover, the NTP treatment showed an insignificant effect on the pore characteristics (Supplementary Fig. 4 and Supplementary Table 1), whereas it enhanced the bulk crystallinity of the resulting HKUST-1 compared to the pristine sample, as evidenced by the post plasma treatment XRD analysis (Supplementary Figs. 5–7). Defects such as extra-framework guests (e.g. H_2O and solvents) and ligand dislocations[24, 25, 26] are known to be present in MOFs, causing the poor crystallinity of MOFs[26]. Previous studies showed that short-lived plasma species could be formed inside nm-scale pores of catalysts[27, 28, 29]. Hence, the energetic plasma species (e.g. electrons or ions) are responsible for dissociating H_2O and reacting the unstable organic components (as seen the CO evolution in Fig. 1a as well as the C1s spectra in Supplementary Fig. 8a) from the surface of HKUST-1. It should be noted that CO formation due to plasma decomposition of residual carboxylic acid is expected since they cannot be removed completely by the thermal activation (see Supplementary Note 1, as evidenced by the IR band at slightly above 1,700 cm^{-1} [24] in Supplementary Fig. 9. This treatment resulted in a more crystalline and stable material remaining. The full width at half maximum (FWHM) of (222) reflections of the NTP-treated HKUST-1 MOFs (Fig. 1b) decreased with an increase in the NTP treatment time. Conversely, the net peak height intensity of HKUST-1 (222) reflection peak increased accordingly. Peak width changes due to the crystallite size variation are not likely because SEM analysis showed the crystallite structures intact after the plasma treatment (see Supplementary Figs. 11–13). The NTP treatment also did not alter the chemical oxidation state of Cu sites of HKUST-1, as evidenced by post-treatment X-ray photoelectron spectroscopy (XPS, see Supplementary Fig. 14). Most importantly, the NTP-treated HKUST-1 is notably more stable than the pristine sample as shown in Fig. 1c, also in Supplementary Fig. 15.

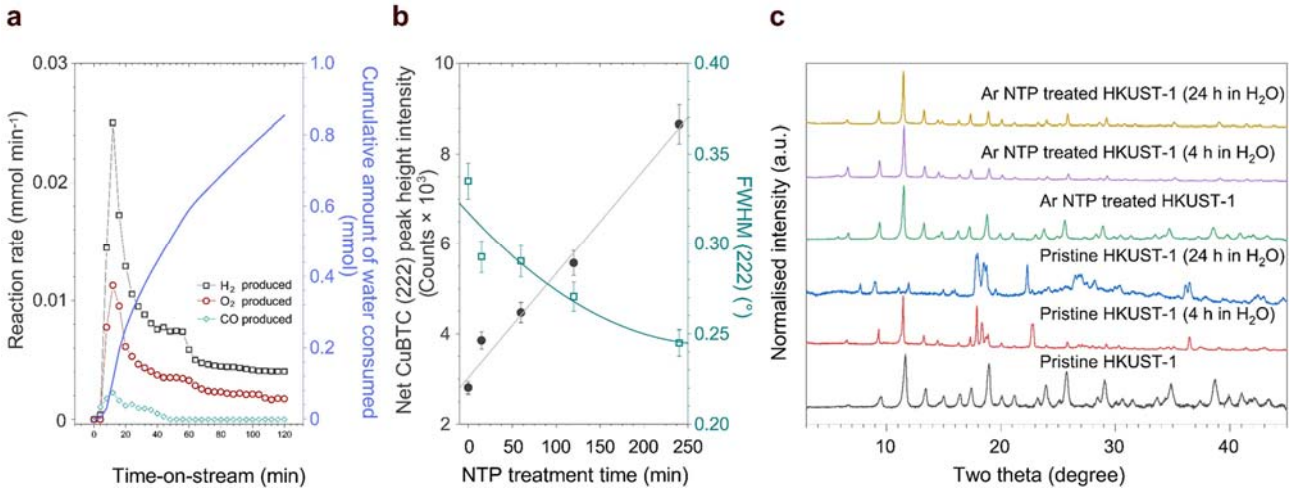

Fig. 1 | Effect of Ar non-thermal plasma treatment on HKUST-1. a, Gas evolution during the Ar plasma (at a specific energy density, SED, of 2 kJ L^{-1}) treatment of wet HKUST-1 (20 vol.% HKUST-1 pellets/80 vol.% $BaTiO_3$ beads packing in a PBP reactor. Dry Ar as the discharge gas), showing the plasma decomposition of water and residual carboxylic acid. **b**, The peak height and FWHM of (222) face of HKUST-1 as a function of NTP treatment time, showing the effect of the plasma treatment on the crystalline structure of HKUST-1. **c**, XRD patterns of the pristine HKUST-1 and Ar plasma treated HKUST-1 (at an SED of 2 kJ L^{-1} for 240 min) after the water stability test at different soaking times (volume ratio: HKUST-1:Water = 1:2), showing the improved stability of Ar plasma treated HKUST-1. Error bars correspond to the average taken over at least three independent measurements.

NTP activated HKUST-1 catalysed WGSR. The uniform distribution of open Cu sites and their selective binding to water and CO[30] in HKUST-1, coupled with its excellent stability in Ar plasma, motivated us to study the WGSR catalysed by HKUST-1. We investigated the catalytic performance of various PB systems (i.e. $BaTiO_3$, HKUST-1 and 3A zeolite packings as shown in Supplementary Fig. 1) under thermal and NTP activation. Under NTP activation, when HKUST-1 was tested, $BaTiO_3$ with a high dielectric constant was used (80 vol.%) to dilute the packing in order to mitigate the effect of the difference in the dielectric constants of materials (ε_{BaTiO_3} = 10,000 vs. $\varepsilon_{HKUST\text{-}1}$ < 10) on the electrical characteristic of different PBP reactors. A control NTP experiment with hydrophilic 3A zeolite packing (with 80 vol.% $BaTiO_3$ beads) was also performed to demonstrate the effect of bed hydrophilicity on the NTP-assisted WGSR.

The PBP reactors were operated at 25 °C without external heating. However, the ignition of the plasma led to an increase in the reactor temperature (to ca. 100 °C measured by an IR thermometer), which was due to the effect of Joule heating rather than the exothermicity of WGSR[12]. The thermal effect of NTP on WGSR was insignificant, as evidenced by the low CO conversion of 2% at 100 °C using pure $BaTiO_3$ PB (Fig. 2a). Over the $BaTiO_3$ PBP with the NTP activation, the CO conversion increased by ten-fold to ca. 21.1%. The catalytic effect of OMSs in HKUST-1 in the WGSR was obvious when the HKUST-1 packing was used in the NTP system (Fig. 2a). Under thermal activation, low activity (Fig. 2b) and severe decomposition of HKUST-1 (see Supplementary Fig. 16) in the WGSR were observed, showing a low CO conversion of about 5.5% and the peculiar high CO_2 selectivity of the thermal-HKUST-1 system as a function of time-on-stream, ToS (Fig. 2c). The highest conversion of CO was achieved using the NTP-assisted HKUST-1-WGSR system of ca. 43.0% corresponding to an effective turnover frequency (TOF_E) value of 8.8 h^{-1} (accessible Cu OMSs were determined by CO titration, as shown in Supplementary Fig. 17 and Supplementary Tables 2 and 3, and discussed in Supplementary Note 2), outperforming the state-of-the-art supported Cu and Cu-based mixed oxide catalysts (e.g. 0.026 h^{-1} at 120 °C, Supplementary Table 2)[31, 32]. Although the CO conversion in the NTP system is ~8 times higher than that obtained by the thermal activation, the values of TOF_E of the two systems are comparable (see Supplementary Tables 3 and 4), indicating that the NTP activation does not change the catalyst (i.e. HKUST-1) or the reaction pathway. NTP treatment rendered more Cu OMSs available for binding CO than was possible following thermal activation of the pristine HKUST-1 by approximately a tenfold increase (see Supplementary Tables 3 and Supplementary Note 2). However, importantly the nature of the site did not change as shown by the XPS data indicating the presence of Cu(II) in the OMSs (Supplementary Fig. 14). It should be noted that it is challenging to decouple the effects of the plasma in terms of the active site and the gas phase processes, for example, as these all contribute to the overall activity measured. The plasma required about 30 min to stabilise, resulting in a slow increase in CO conversions in all the PBP systems (Fig. 2b). Under

steady state conditions, among the catalytic systems studied, NTP-HKUST-1-WGSR showed a comparatively superior performance over the others systems studied over 240 min ToS. In addition, the CO_2 selectivities under steady-state conditions of the inert $BaTiO_3$ PBP were ca. 82.5%, whereas that of HKUST-1 packing was close to 99.0%.

Roles of Cu OMSs and NTP in catalytic WGSR. The synergy between OMSs in HKUST-1 and NTP activation lead to the enhanced performance of the WGSR through (i) the intensified NTP-induced water dissociation due to the hydrophilic OMSs and (ii) the intrinsic catalytic role of Cu OMSs in the WGSR. The WGSR requires hydroxyl radicals (OH) for surface CO oxidation[33], via the associative pathway[34, 35]. We found that the CO conversion in the NTP-WGSR was favoured by the PB's hydrophilicity. We supported this claim using a control NTP experiment with a 3A zeolite packing (with high hydrophilicity, Supplementary Fig. 18), in which a CO conversion of 28.7% was observed (see Supplementary Fig. 19), enhanced by 36% in comparison to the inert $BaTiO_3$ PBP. In situ optical emission spectroscopic (OES) examination of the NTP-catalysis systems are depicted in Fig. 2d, in which the OH electronic emission at 308 nm ($A^2\ \Sigma^+ \rightarrow X^2\prod$) and Ar I emission were observed in all the plasma systems. The intensity and intensity distribution of Ar I emission lines (Fig. 2d) from three PBP reactors is of the same order of magnitude (10^3), suggesting that their electron temperatures and plasma characteristics can be considered as similar to a first approximation. In comparison to the control experiments with $BaTiO_3$ and 3A PBs, a much higher intensity of OH radicals was seen in the NTP-HKUST-1-WGSR, corresponding to a higher OH concentration in the gas phase and higher electron energy. It thus confirms that the NTP-HKUST-1-WGSR system is able to dissociate water to release OH radicals in the gas phase (possibly on the surface of OMSs as well), which subsequently react with CO on OMSs to form surface intermediates before releasing CO_2[33]. Since the water dissociation on Cu OMSs in HKUST-1 under thermal activation is highly challenging, the availability of gas phase OH enabled by NTP is the key to activate the WGSR in the presence of HKUST-1.

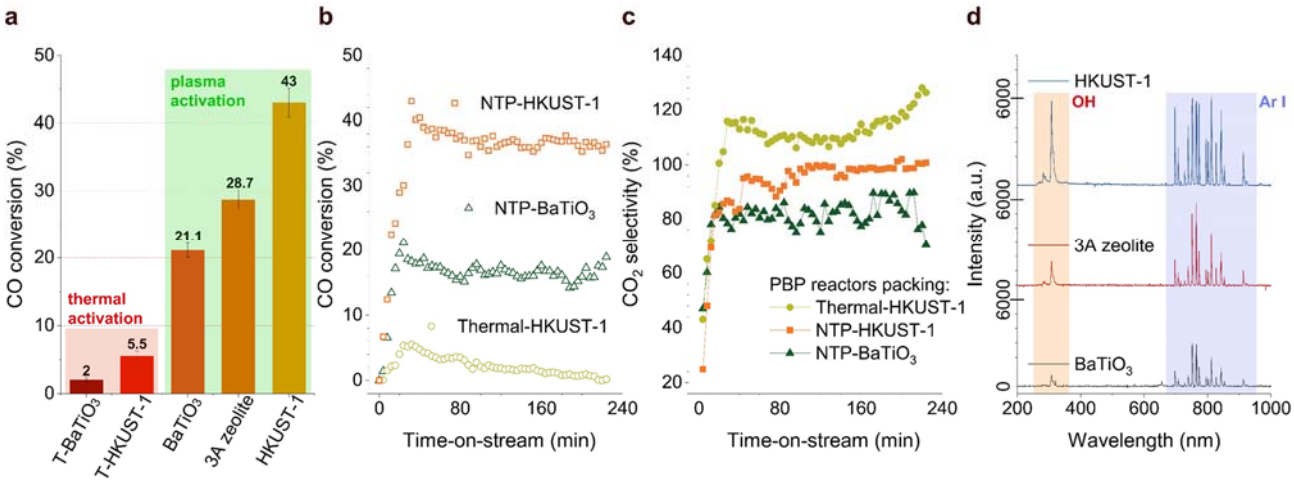

Fig. 2 | Catalytic water-gas shift reaction (WGSR) by thermal and NTP activation. a, CO conversions of the WGSR for PB reactors (HKUST-1 and 3A packing were diluted using 80 vol.% $BaTiO_3$) by thermal (at 100 °C) and NTP activation, showing the positive effect of the bed hydrophilicity on WGSR under NTP and the improved catalysis in the NTP-HKUST-1-WGSR system. **b**, OES spectral lines of plasma for different packings at a discharge power of 8.6 W, showing the positive effect of the bed hydrophilicity on dissociating water to release OH radicals under NTP. **c**,**d**, Corresponding catalytic performance for different PB reactors as a function of ToS, showing the comparison of the catalytic activity of various systems. (**c**) CO conversions and (**d**) CO_2 selectivities (CH_4 was not detected by GC, Supplementary Fig. 20). NTP system: SED = ca. 3.4 kJ L^{-1}; gas feed = 0.7% CO and 2.8% H_2O in Ar, total flow rate = 150 mL min^{-1}. Error bars correspond to the average taken over at least three independent measurements.

The interaction between Cu OMSs and substrate molecules (CO) was evidenced by ex situ XPS study of Cu OMSs near the surface of HKUST-1 (ca. 10 nm depth of analysis, see Supplementary Fig. 21 and Supplementary Note 3) before and after the NTP-HKUST-1-WGSR and in situ DRIFTS analysis of CO adsorption on HKUST-1 (see Supplementary Fig. 22), showing the occurrence of Cu(I) due to the CO-induced auto-reduction of Cu(II) to Cu(I) sites in HKUST-1[36]. By performing in situ DRIFTS analysis for the NTP-HKUST-1-WGSR (see Supplementary Figs. 23 and 24), the catalytic role of Cu OMSs of HKUST-1 in the NTP system was confirmed. Fig. 3a shows that, prior to the ignition of Ar plasma, in the CO absorption region of 2,250–2,000 cm^{-1}, a strong feature at 2,110 cm^{-1} corresponding to the Cu(I)-adsorbed carbonyl species was observed. Upon the ignition of plasma, this band shifted to higher wavenumber by about 15 cm^{-1} relative to the Cu(II)-CO band. This was clearest under high plasma power conditions (e.g. 2,125 cm^{-1} at 6 kV

and 22.5 kHz, corresponding to the SED of 3.5 kJ L^{-1}), revealing the Cu(II)/Cu(I) redox interplay during the WGSR.

Most importantly, the ignition of plasma caused the almost instantaneous appearance of surface species at the expense of some adsorbed CO, as presented in Fig. 3b, indicating the possible OCO asymmetric (1,575 cm^{-1}) and symmetric (1,390 cm^{-1}) stretching vibrations (similar to the formates on metal oxides[37, 38, 39]). In addition, by increasing the plasma power, stronger IR bands of surface species in the wavenumber range 1,800−1,100 cm^{-1} were measured which are likely to be due to surface carbonates[40]. This increase in the surface species may be the origin of the enhancement observed in the plasma-assisted MOFs surface catalysed WGSR. Therefore, based on the in situ DRIFT spectroscopic data, the significant evolution of the IR bands due to the adsorbed surface intermediates during NTP-HKUST-1-WGSR supports the assertion that the OMSs in HKUST-1 enable the heterogeneous reaction pathways during the WGSR with the role of the NTP to aid the dissociation of water which (i) maintains the stability and activity of HKUST-1 and (ii) eliminates one of the rate-limiting step by providing the hydroxyl intermediate from the gas phase.

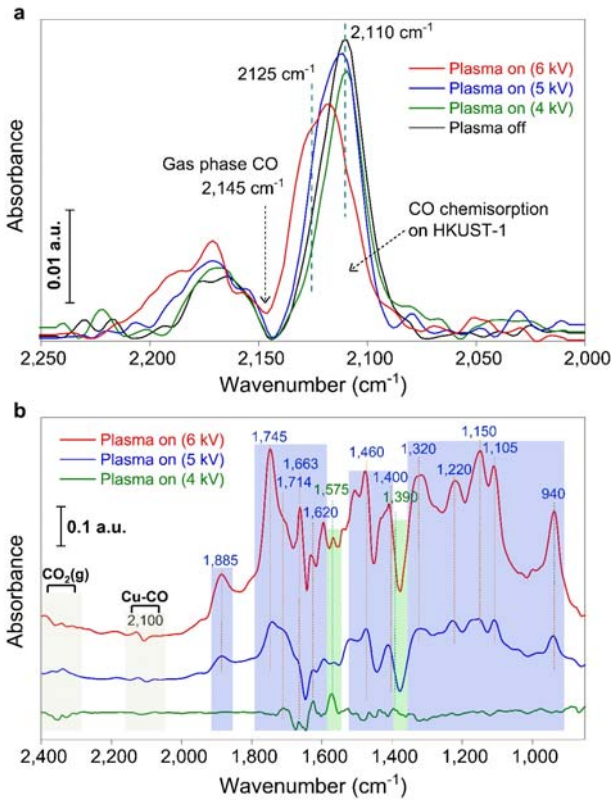

Fig. 3 | In situ DRIFTS characterisation. a, In situ DRIFTS spectra of CO adsorbed on Cu OMSs in HKUST-1 under NTP, showing the plasma effect on HKUST-1 during the NTP treatment. **b**, In situ DRIFTS spectra of HKUST-1 in the NTP-assisted WGSR at different plasma discharge powers, showing the plasma effect on surface species during the reaction. NTP system: SED = 1.6, 2.5 and 3.5 kJ L^{-1}; gas feed = 0.7% CO and 2.8% H_2O in Ar, total flow rate = 150 mL min^{-1}, room temperature. All spectra were background subtracted using the spectrum before the plasma ignition.

Mechanism and stability. In contrast with the nature of the active sites in conventional supported metal catalysts, such as Cu/Al_2O_3, Au/CeO_2 and Pt/TiO_2[31, 32], two adjacent Cu OMSs in HKUST-1 are thought to form the catalytically active centres for the WGSR[7, 8]. Therein, Cu(II)/Cu(I) entities are established with the presence of CO, resulting in the preferential binding of CO to the Cu(I) sites. The plasma species dissociate the gas phase and OMSs-bound H_2O into H and OH, which overcome (i) the rate-limiting step in the WGSR[41] and (ii) the hydrothermal instability of Cu(II) OMSs at elevated temperatures, providing a ready supply of OH to promote the formation of the

surface species, and hence activate the WGSR via the heterogeneous surface pathway (see Supplementary Figs. 25–26, Supplementary Note 5).

By conventional thermal activation, WGSR requires at least 150 °C to activate the Cu catalysts for CO conversion[31, 32, 42], however, under these conditions, the HKUST-1 cannot survive due to the presence of water vapour. In contrast, using NTP activation under ambient conditions, HKUST-1 shows surprisingly high CO conversion of 43% (corresponding to a TOF of 8.8 h^{-1} vs. <2.6×10^{-2} h^{-1} by supported Cu and Cu-based mixed oxide catalysts[31, 32] at comparable temperatures, Supplementary Table 2), as well as sustained activity under the humid conditions. Post the NTP-HKUST-1-WGSR, the structure of HKUST-1 was not significantly altered, as shown by XRD and XPS, N_2 physisorption, FT-IR and dynamic water vapour sorption characterisation of used materials (Fig. 4, Supplementary Figs. 27–29), demonstrating the high stability of HKUST-1. In addition to the specific case with HKUST-1, WGSR experiments over other Cu MOFs such as Cu-MOF-74 and $Cu(bdc)(ted)_{0.5}$ MOFs were also performed to demonstrate the generic nature of the NTP-MOFs system developed (see Supplementary Figs. 30–33, Supplementary Table 5 and Supplementary Note 6).

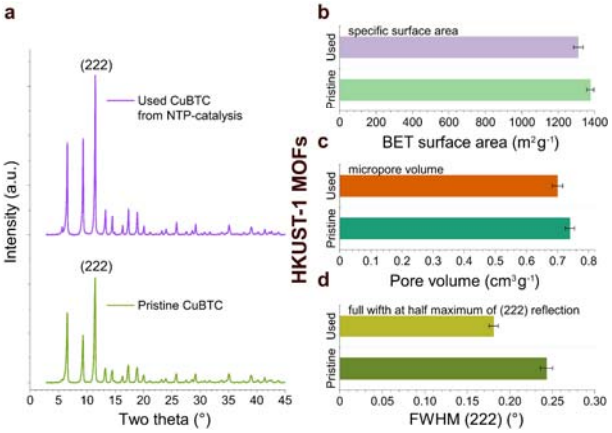

Fig. 4 | Comparison of the pristine and used HKUST-1 by PXRD and N_2 physisorption. a, PXRD patterns of the pristine and used HKUST-1. **b**, Specific surface areas of the pristine and used HKUST-1 by N_2 physisorption. **c**, micropore volumes of the pristine and used HKUST-1 by N_2 physisorption. **d**, FWHM of (222) reflection of the pristine and used HKUST-1.The used HKUST-1 was from the NTP-HKUST-1-WGSR at ca. 3.4 kJ L^{-1} after 240 min ToS; gas feed: 0.7% CO and 2.8% H_2O in Ar. All figures show the insignificant

change in the structure of HKUST-1 post the NTP-WGSR. Error bars correspond to the average taken over at least three independent measurements.

Discussion

The most challenging feature of using MOFs in heterogeneous catalysis lies in the role of OMSs, which have to provide a balance between activity and stability during the reaction under heating or the presence of water or both. We have investigated the behaviour of a MOF during the challenging WGSR assisted by NTP. Cu OMSs in HKUST-1, showed excellent catalytic activity for the WGSR under NTP conditions. The plasma promoted the dissociation of H_2O supplying OH to enable the WGSR, as well as preventing the water-induced decomposition of HKUST-1, resulting in an enhanced stability. In a packed bed reactor under plasma conditions, the substitution of 20 vol.% of $BaTiO_3$ packing with HKUST-1 pellets resulted in a >100% enhancement in the CO conversion. The developed NTP assisted MOFs-WGSR (TOF = 8.8 h^{-1}) surpassed the TOFs achieved by state-of-the-art Cu catalysts at comparable temperatures (0.026 h^{-1})[31, 32, 42]. Moreover, the NTP-MOFs-WGSR also showed a good performance using a low H_2O/CO ratio of 1–4, reducing the steam and energy which are conventionally used in practical settings[43, 44]. Additionally, the stability enhancement of MOFs induced by plasma treatment proved as general phenomenon, as evidenced using HKUST-1 in combination with various SEDs and discharge gases, as well as using Cu-MOF-74 or $Cu(bdc)(ted)_{0.5}$ MOFs with Ar plasma (see Supplementary Figs. 6, 30 and 32 and Supplementary Note 6). More importantly, we also showed that NTP improves the catalytic activity of different Cu MOFs towards WGSR (namely Cu-MOF-74 and $Cu(bdc)(ted)_{0.5}$, see Supplementary Figs. 30–33 and Supplementary Note 6), further corroborating the generality of the approach. NTP-catalytic systems are highly complex and involve the interaction of vibrationally and electronically excited species, radicals, electrons or photons produced by the plasma discharge in the gas phase with the catalyst surface and adsorbed molecules[13]. MOFs with well-isolated and uniform single

OMSs, i.e. with minimal variation in the physical and chemical properties are therefore ideal platforms to gain insight into NTP-catalysis.

Methods

Catalyst testing. The NTP treatment of MOFs and NTP-WGSRs were performed in a packed-bed plasma (PBP) reactor (Supplementary Fig. 1, $BaTiO_3$ beads as the main packing material at atmospheric pressure). A detailed description of the PBP reactor and its plasma power supply system has been described elsewhere[23]. For the NTP treatment, pure Ar gas was used as the discharge gas at a specific energy density (SED) of 2 kJ L^{-1} and commercial HKUST-1 pellets were used. HKUST-1 pellets were obtained from MOF technologies Ltd. (UK) and used as received. HKUST-1 pellets were packed into the PBP reactor (20 vol.% with 80 vol.% $BaTiO_3$) for the Ar plasma treatment at an SED of 2 kJ L^{-1}. Prior to the catalytic tests, HKUST-1 was activated at 120 °C overnight to remove any remaining H_2O and organic solvent from the framework.

The WGSR was performed using 0.7% CO (99.99%) and 2.8% H_2O in Ar (99.9%) balance gas mixture at 150 mL min^{-1} total gas flow rate and 25 °C. Gas delivery of CO and Ar was controlled by mass flow controllers (MKS Instruments). CO/Ar mixture was passed through a water bubbler to introduce saturated water vapour at 25 °C. The plasma was enabled by an AC neon sign transformer (10 kV, 30 mA and 21 kHz), with a Variac (Zenith Electric Company Ltd.) supplying the input voltage and thus a controllable output voltage. A high voltage probe (TES TEC HVP–15HF) and a current probe (Pearson™ current monitor model 411 were connected to a Pico scope (Pico Technology ADC-216) to characterise the supplied power. The plasma input power was around 8.6 W and the specific energy density was around 3.4 kJ L^{-1}. The temperature of the PBP reactor was monitored using an IR thermometer (IRT670, General Tools & Instruments).

The visible light emission from the plasma in the PBP reactor was monitored using optical emission spectroscopy (OES). The spectrometer (USB2000+, Ocean Optics) had a wavelength

range from 180 to 1100 nm and a 1.4 nm FWHM spectral resolution. The lens was placed close to the centre of the quartz reactor axis and at a distance to maximise the collected light emission from the PBP reactor. About 40 s was used to average the data collected as the visible emission was generally weak. At least three spectra were collected then averaged to give the final readings.

Prior to the WGSR, HKUST-1/$BaTiO_3$ and 3A/$BaTiO_3$ packings were treated with dry Ar plasma for 4 h to remove the adsorbed water. The 3A zeolite was used as the benchmark packing for comparative study due to the strong affinity of the zeolite to H_2O as also found for HKUST-1, while water adsorption on $BaTiO_3$ was negligible compared to HKUST-1 and 3A zeolite. Thermal activation of the packed bed reactor with $BaTiO_3$ and HKUST-1/$BaTiO_3$ packings at 100 °C was also carried out (under the same gas feed) to compare the catalytic performance by different activation modes.

The analysis of gaseous products (CO_2, CO, O_2 and H_2) from the PBP reactor was carried out using a two-channel micro-gas chromatograph (Agilent 3000A). Each channel was equipped with a thermal conductivity detector (TCD). One channel measured CO and O_2 using a molecular sieve 5A column, and the other measured the H_2 and CO_2 using a Poraplot Q column. The typical GC patterns of the results are shown in Supplementary Fig. 20. The CO conversion and the CO_2 selectivity were calculated using equation 1 and equation 2, respectively. Each point was an average of three consecutive measurements, with standard errors of ± 2.60% for CO conversion and ± 2.00% for CO_2 selectivity, respectively.

$$X_{CO} = \frac{[CO]_{inlet} - [CO]_{outlet}}{[CO]_{inlet}} \times 100\% \quad (1)$$

$$S_{CO_2} = \frac{[CO_2]_{outlet}}{[CO]_{inlet} - [CO]_{outlet}} \times 100\% \quad (2)$$

In situ DRIFTS analysis. The in situ DRIFT measurements of CO adsorption on HKUST-1 were carried out using a Bruker Vertex 70 FTIR spectrometer equipped with a liquid N_2 cooled detector.

The spectra were recorded at 4 cm^{-1} resolution and each spectrum was averaged 256 times. The sample was first activated at 120 °C under argon (Ar, 99.999%, BOC gas Ltd.) for 4 h in order to remove adsorbed water and other gas molecules. Then the temperature of the sample was reduced to room temperature. The spectrum of the activated sample at room temperature was used as the background reference for the following adsorption experiments. To probe the CO adsorption on the activated HKUST-1 at room temperature, 5% CO (in Kr, total flow rate = 50 ml min^{-1}) was first introduced to the DRIFTS cell to establish the saturated CO peaks, and then the gas was switched to pure Ar (total flow rate = 50 ml min^{-1}) to purge the sample to reveal the CO binding on OMSs.

The in situ DRIFT measurements of the WGSR over HKUST-1 under plasma were measured using a Bruker Tensor 70 FTIR spectrometer (resolution = 4 cm^{-1}) using a specifically designed in situ plug flow cell with the plasma generated in the catalyst bed using a modified Spectra Tech Collector II DRIFTS accessory (Supplementary Fig. 23). All spectra were measured under steady states and each spectrum was averaged 128 times. The catalyst was first activated at 120 °C under Ar (99.999%, BOC gas Ltd.) for 4 h in order to remove adsorbed water and other gas molecules. Then the temperature of the sample was reduced to room temperature. The spectrum of the annealed sample at room temperature was used as the background reference for the following WGSR. The WGSR was performed using 0.7% CO (99.99%) and 2.8% H_2O in Ar (99.9%) balance gas mixture at 150 ml min^{-1} total gas flow rate and 25°C. Gas delivery of CO and Ar was controlled by mass flow controllers (MKS Instruments). CO/Ar mixture was passed through a water bubbler to introduce the saturated water vapour at 25 °C. The plasma generator was an alternating current power source (PVM500 model) as used in our previous report[12] and the electrical parameters were monitored using an oscilloscope (Tektronix TBS1062) that was connected to the reactor through a high voltage probe (Tektronix, P6015). The applied voltages were 4, 5, 6 kV (unless otherwise stated) at a frequency of 22.5 kHz.

Materials characterisation. Powder X-ray diffraction (XRD) of materials was carried out using a PANalytical X'Pert Pro X-ray diffractometer. The radiation source was Cu $K\alpha_1$ with a wavelength

of 1.5405 Å. The diffractograms were recorded from 3° to 46 ° with a step size of 0.017°. To obtain high-resolution XRD patterns of materials, the diffractograms were recorded from 3° to 50° with a step size of 0.002°, with about 11 h scan time. The high-resolution XRD diffractograms were used for Pawley fitting and Rietveld refinement.

N_2 physisorption was carried out at 77 K with a Micrometrics ASAP 2020 analyser to characterise the porous structure of the materials studied. Before the N_2 sorption measurement, the materials were outgassed at 90 ºC overnight under vacuum. The specific surface area of the materials was determined based on the Brunauer-Emmett-Teller (BET) method. Single point adsorption total pore volume was determined at $p/p^0 = 0.99$.

CO titration of accessible Cu OMSs in HKUST-1. Temperature programmed desorption (TPD) of CO from HKUST-1 was performed to determine the number of available and accessible sites for binding CO to the Cu OMSs. The sample was placed into a quartz tube reactor of the TPD instrument equipped with mass spectrometry (MS, Hiden Analytical, HPR-20 QIC) for gas analysis and was first activated at 120 °C under Ar at 100 ml min^{-1} (99.999%, BOC gas Ltd.) for 20 h in order to remove adsorbed guest molecules. After the activation, the temperature of the sample was decreased to 30 °C and the temperature maintained until a stable MS baseline signal was achieved. Then a gas mixture of 0.7% CO and 0.7% krypton (Kr) balanced in Ar (total flow rate = 100 ml min^{-1}) was introduced to establish the saturated CO signal (after 3 h gas adsorption at 30 °C). The gas was switched to pure Ar (at 100 ml min^{-1}) to purge the physical adsorbed CO from the sample as noted when the baseline signal of gases from MS became stable. The temperature of the reactor was increased at a rate of 10 °C min^{-1} in pure Ar to measure the CO desorption. Kr was used as the internal standard gas to calibrate the dead volume of the TPD system. A feed of 0.7% CO was used to calibrate the mass 28 signal in the MS. To assess the surface coverage, it was assumed that one CO molecule adsorbs on each Cu site. Two samples were used in the CO titration experiment, i.e. the thermally activated HKUST-1 (at 120 °C under Ar) and the Ar plasma (NTP) activated HKUST-1 (SED = 2 kJ L^{-1}, duration = 240 min).

Data availability

All figures presented in this paper are associated with raw data. The data that support the plots within this paper and other findings of this study are available from the corresponding author upon reasonable request.

References

1. Yaghi, O. M. & Li, H. Hydrothermal synthesis of a metal-organic framework containing large rectangular channels. J. Am. Chem. Soc. **117**, 10401–10402 (1995).

2. Corma, A. et al. Engineering metal organic frameworks for heterogeneous catalysis. Chem. Rev. **110**, 4606–4655 (2010).

3. Rowsell, J. L. C. & Yaghi, O. M. Metal–organic frameworks: a new class of porous materials. Microporous Mesoporous Mater. **73**, 3–14 (2004).

4. Peterson, V. K. et al. Neutron powder diffraction study of D_2 Sorption in Cu_3(1,3,5-benzenetricarboxylate)$_2$. J. Am. Chem. Soc. **128**, 15578–15579 (2006).

5. Chui, S. S. et al. A chemically functionalizable nanoporous material $[Cu_3(TMA)_2(H2O)_3]_n$, Science **283**, 1148–1150 (1999).

6. Al-Janabi, N. et al. Mapping the Cu-BTC metal–organic framework (HKUST-1) stability envelope in the presence of water vapour for CO_2 adsorption from flue gases. Chem. Eng. J. **281**, 669–677 (2015).

7. Alaerts, L. et al. Probing the Lewis acidity and catalytic activity of the metal-organic framework $[Cu_3(btc)_2]$ (BTC=Benzene-1,3,5-tricarboxylate). Chem. Eur. J. **12**, 7353–7363 (2006).

8. Luz, I. et al. Bridging homogeneous and heterogeneous catalysis with MOFs: Cu-MOFs as solid catalysts for three-component coupling and cyclization reactions for the synthesis of propargylamines, indoles and imidazopyridines. J. Catal. **285**, 285–291 (2012).

9. Al-Janabi, N. et al. Underlying mechanism of the hydrothermal instability of $Cu_3(BTC)_2$ metal-organic framework. Front. Chem. Sci. Eng. **10**, 103–107 (2016)

10. Al-Janabi, N. et al. Cyclic adsorption of water vapour on CuBTC MOF: Sustaining the hydrothermal stability under non-equilibrium conditions. Chem. Eng. J. **333**, 594–602 (2018).

11. Mehta P. et al. Overcoming ammonia synthesis scaling relations with plasma-enabled catalysis. Nat. Catal. 2018, **1**, 269–275 (2018).

12. Stere, C. E. et al. Non-thermal plasma activation of gold-based catalysts for low-temperature water-gas shift catalysis. Angew. Chem. Int. Ed. **56**, 5579–5583 (2017).

13. Gibson, E. K. et al. Probing the role of a non-thermal plasma (NTP) in the hybrid NTP catalytic oxidation of methane. Angew. Chem. Int. Ed. **56**, 9351–9355 (2017).

14. Ashford, B. & Tu, X. Non-thermal plasma technology for the conversion of CO_2. Curr. Opin. Green Sustainable Chem. **3**, 45–49 (2017).

15. Bae, J. et al. Oxygen plasma treatment of HKUST-1 for porosity retention upon exposure to moisture. Chem. Commun. **53**, 12100–12103 (2017).

16. Luo, J. et al. Water splitting in low-temperature ac plasmas at atmospheric pressure. Res. Chem. Intermed. **26**, 849–874 (2000).

17. Decoste, J. B. et al. Enhanced stability of Cu-BTC MOF via perfluorohexane plasma-enhanced chemical vapor deposition. J. Am. Chem. Soc. **134**, 1486–1489 (2012).

18. Decoste, J. B. et al. Hierarchical pore development by plasma etching of Zr-based metal-organic frameworks. Chem. Eur. J. **21**, 18029–18032 (2015).

19. Sadakiyo, M. et al. A new approach for the facile preparation of metal-organic framework composites directly contacting with metal nanoparticles through arc plasma deposition. Chem. Commun. **52**, 8385–8388 (2016).

20. Tao, L. et al. Creating coordinatively unsaturated metal sites in metal-organic-frameworks as efficient electrocatalysts for the oxygen evolution reaction: Insights into the active centers. Nano Energy **41**, 417–425 (2017).

21. Bahri M. et al. Metal organic frameworks for gas-phase VOCs removal in a NTP-catalytic reactor. Chem. Eng. J. **320**, 308-318 (2017).

22. Junliang W. et al. Chromium-based metal-organic framework MIL-101 as a highly effective catalyst in plasma for toluene removal. J. Phys. D Appl. Phys. **50**, 475202 (2017).

23. Xu, S. et al. CO_2 conversion in a non-thermal, barium titanate packed bed plasma reactor: The effect of dilution by Ar and N_2. Chem. Eng. J. **327**, 764–773 (2017).

24. Drenchev N. et al. CO as an IR probe molecule for characterization of copper ions in a basolite C300 MOF sample. Phys. Chem. Chem. Phys. **12**, 6423–6427 (2010).

25. Al-Janabi, N. et al. Assessment of MOF's quality: Quantifying defect content in crystalline porous materials. J. Phys. Chem. Lett. **7**, 1490–1494 (2016).

26. Cheetham, A. K. et al. Defects and disorder in metal organic frameworks. Dalton Trans. **45**, 4113–4126 (2016).

27. Holzer, F. et al. Combination of non-thermal plasma and heterogeneous catalysis for oxidation of volatile organic compounds: Part 1. Accessibility of the intra-particle volume. Appl. Catal. B Environ. **38**, 163–181 (2002).

28. Roland, U. et al. Combination of non-thermal plasma and heterogeneous catalysis for oxidation of volatile organic compounds: Part 2. Ozone decomposition and deactivation of γ-Al_2O_3. Appl. Catal. B Environ. **58**, 217–226 (2005).

29. Zhang, Y. R. et al. Can plasma be formed in catalyst pores? A modeling investigation. Appl. Catal. B Environ. 2016, **185**, 56–67 (2016).

30. Karra, J. R. & Walton, K. S. Effect of open metal sites on adsorption of polar and nonpolar molecules in metal-organic framework Cu-BTC. Langmuir **24**, 8620–8626 (2008).

31. Jeong, D.-W. et al. Low-temperature water–gas shift reaction over supported Cu catalysts. Renew. Energy **65**, 102–107 (2014).

32. Tanaka, Y. et al. Water gas shift reaction over Cu-based mixed oxides for CO removal from the reformed fuels. Appl. Catal. A Gen. **242**, 287–295 (2003).

33. Gokhale, A. A. et al. On the mechanism of low-temperature water gas shift reaction on copper. J. Am. Chem. Soc. **130**, 1402–1414 (2008).

34. Aranifard, S. et al. On the importance of the associative carboxyl mechanism for the water-gas shift reaction at Pt/CeO_2 interface sites. J. Phys. Chem. C **118**, 6314–6323 (2014).

35. Burch, R. Gold catalysts for pure hydrogen production in the water-gas shift reaction: activity, structure and reaction mechanism. Phys. Chem. Chem. Phys. **8**, 5483–5500 (2006).

36. Szanyi, J. Well-studied Cu-BTC still serves surprises: evidence for facile Cu^{2+}/Cu^{+} interchange. Phys. Chem. Chem. Phys. **14**, 4383–4390 (2012).

37. Chen, C.-S. et al. Active sites on Cu/SiO_2 prepared using the atomic layer epitaxy technique for a low-temperature water–gas shift reaction. J. Catal. **263**, 155–166 (2009).

38. Ilinich, O. et al. Cu–Al_2O_3–$CuAl_2O_4$ water–gas shift catalyst for hydrogen production in fuel cell applications: Mechanism of deactivation under start–stop operating conditions. J. Catal. **247**, 112–118 (2007).

39. Wang, X. et al. In situ studies of the active sites for the water gas shift reaction over Cu−CeO_2 catalysts: Complex interaction between metallic copper and oxygen vacancies of ceria. J. Physi. Chem. B **110**, 428–434 (2006).

40.Du, H. et al. In situ FTIR spectroscopic analysis of carbonate transformations during adsorption and desorption of CO_2 in K-Promoted HTlc. Chem. Mater. **22**, 3519–3526 (2010).

41. Campbell, C. T. & Daube, K. A. A surface science investigation of the water-gas shift reaction on Cu(111). J. Catal. **104**, 109–119 (1987).

42. Zhang, Z. et al. The most active Cu facet for low-temperature water gas shift reaction. Nature Commun. **8**, 488 (2017).

43. Baier, T. & Kolb, G. Temperature control of the water gas shift reaction in microstructured reactors. Chem. Eng. Sci. **62**, 4602–4611 (2007).

44. Łaniecki, M. et al. Water–gas shift reaction over sulfided molybdenum catalysts. Appl. Catal. A Gen. **196**, 293–303 (2000).

Acknowledgements

X.F. thank the financial support from The Royal Society (RG160031). P.A.M. and S.X. gratefully acknowledge the support from the European Community's Seventh Framework (FP7)/People-Marie Curie Actions Programme (RAPID under Marie Curie Grant agreement no 606889). The UK Catalysis Hub is kindly thanked for resources and support provided via our membership of the UK Catalysis Hub Consortium and funded by EPSRC (Portfolio Grants. EP/K014706/2, EP/K014668/1, EP/K014854/1, EP/K014714/1 and EP/I019693/1). We thank Dr Sihai Yang, Dr Alex Walton, Dr Rachel Saunders and Dr Thomas Vetter for the kind advice and help on improving the manuscript.

Author contributions

X.F. and S.X. conceived the idea. S.X. designed the NTP reactor under the guidance of P.A.M; carried out the catalytic tests and characterisation of materials using N_2 sorption, XRD, SEM, FT-IR under the guidance of X.F.; performed in situ DRIFTS experiments and data analysis; and the initial discussion of data under the guidance of X.F. and P.A.M. C.S. and S.C. designed and performed the in situ DRIFTS experiments and discussed the data with S.X. under the guidance of C.H. and X.F. K.W., B.I. and A.G. developed the in situ DRIFTS flow cell in collaboration with C.H. S.F.R.T. performed the XPS characterisation and analysis under the guidance of C.H. N.A.J. helped the

dynamic water vapour adsorption experiments under the guidance of X.F. X.F wrote the manuscript. All the authors contributed to the preparation of the manuscript.

Competing interests

The authors declare no competing interests.

Additional information

Supplementary information accompanies this paper at http://www.nature.com/naturecatalysis

Correspondence and requests for materials should be addressed to X.F., P.A.M. and C.H.